

# Retinal glial cells enhance human vision acuity

A. M. Labin and E. N. Ribak

Physics Department, Technion - Israel Institute of Technology, Haifa 32000, Israel

Received January 11, 2010

We construct a light-guiding model of the retina outside the fovea, in which an array of glial (Muller) cells permeates the depth of retina down to the photoreceptors. Based on measured refractive indices, we propagate light to obtain a significant increase of the intensity at the photoreceptors. For pupils up to 6 mm width, the coupling between neighboring cells is only a few percent. Low cross-talk over the whole visible spectrum explains also the insensitivity to chromatic aberrations of the eye. The retina is revealed as an optimal structure designed for improving the sharpness of images.

Keywords: vision, retina, acuity, light guiding, mode propagation PACS: 87.19lt, 42.66.Ne

A prominent feature of the human eye is a resolution and light gathering dependence on incidence angle. Light entering the pupil perpendicularly will pass through the vitreous humor and be incident the fovea, which is the thinner sensitive tissue part of the retina. This special location accounts for the highest visual acuity. On the other hand, light hitting the pupil obliquely will be incident on the parafovea, a much thicker and complex region of the retina (Fig. 1). It is made of the nerve fiber, inner and outer plexiform layers (NFL, IPL, OPL), with their nuclei in the ganglion, inner and outer layers (GCL, INL, ONL). The function of the neurons is to differentiate in space and time the acquired information and pass it on to the brain. So before the light reaches the photoreceptors in the parafovea, it must pass through these lateral tissues, which optically distort and scatter the light. Thus the question arises, why is the retina arranged in this seemingly reverse order of tissues, and what effect does it have on acuity?

Previously it was found that the photoreceptors (cones and rods) have a light-guiding quality [1, 2]. Measurements of refractive indices of parafoveal tissue [3], and recently of glial cells [4] show evidence of waveguide properties of the latter. It was suggested that retinal glial cells deliver light

from the inner limiting membrane, where light is first incident on the retina, down to the photoreceptors where light is being absorbed.

While glial cells might have a role in the parafovea light guiding, due to the substantial depth of the six preceding tissue layers ( $\sim 130 \mu\text{m}$ ), in the thinner fovea their effect can be neglected (Fig. 1). The average separation of these cells grows from ten to  $16 \mu\text{m}$  with their distance from the fovea outward [5]. We used cone counts for that, since in humans, each glial cell is attached to one central cone and a number of rods.

Considering these facts, it is intriguing to investigate the affect of the array of glial cells on human vision acuity. Firstly we should consider light guiding efficiency in one cell as a function of an incoming beam. The beam profile is essentially the diffraction pattern of the pupil. The capability of the cell to guide light is determined by the cell diameter and the differences between the indices of refraction of the cell

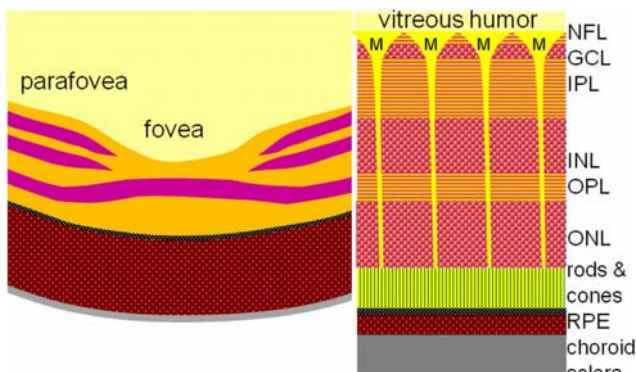


FIG. 1. (Color online) Left: The central 3 mm of the retina. Right: Structure of the parafovea. Nerve layers (horizontal lines) and nuclei (circles) are all transparent, down to the absorbing RPE and choroid. They are permeated by vertical glial cells (M) which are attached to the photoreceptors: rods and cones.

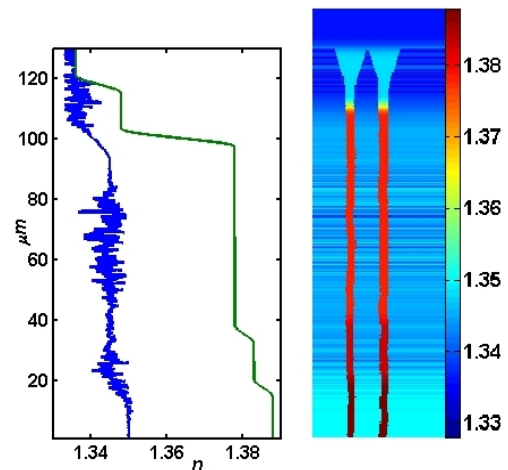


FIG. 2. (Color online) The refractive index structure of the retina. Left: One realization of the refractive index, with fluctuations in the NFL, IPL and OPL higher than in the other tissue layers (blue trace), while the glial refractive index (green) is smoother. Right: Corresponding index structure data-cube. The cell length is  $130 \mu\text{m}$ , and its diameter drops from  $10\text{-}16 \mu\text{m}$  to  $2.4 \mu\text{m}$ . Light was propagated only into the central cell, and diffused to its vicinity.

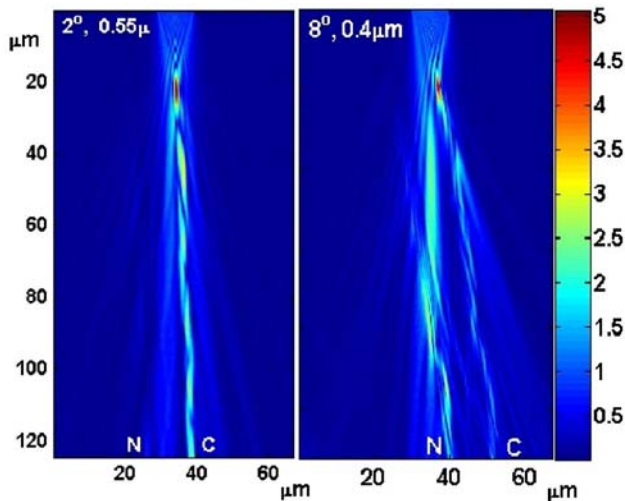


FIG. 3 (Color online). Cuts in field distribution with cells data-cube (Fig. 2) rotated at indicated angles and wave lengths. Notice that some light remains along the incoming direction down the center, but most of it is guided through the central cell C or leaked into the next cell N on the left.

and its surroundings (Fig. 2). The collective quality of the array of glial cells to preserve resolution can only be examined by identifying the interaction between neighboring cells (close neighbors analysis). This interaction is a coupling of electromagnetic fields between parallel cells. If two cells are sufficiently close to each other, energy will transfer from one excited cell to create a signal in its neighbor [6]. Thus it depends on the separation of the cells, the field penetration into the cell and the propagation length. Moreover the special geometry of glial cells [4] also has a crucial role in the interaction. Inter-cell coupling causes loss of resolution and smear of the projected image incident on the retinal surface.

Light traveling along a generic waveguide forms spatial patterns or modes, whose relative strength depends on the incident light. This is usually described by the coupled mode theory [6], and used previously to model light propagation within retinal cones [2]. An analytical description of mode propagation along waveguides such as retinal glial cells must take into account coupling between these pure modes, which are created by imperfections, as core width and refractive index perturbations [3, 4, 7]. However, the complex axial variations of the cells [7] result in significant boundary perturbations, and coupled mode theory is difficult to apply. Instead we used a direct three-dimensional numerical solution of the Helmholtz equation, known as the FFT split-step beam propagation method (BPM) of the global third order. The algorithm is stable and provides a detailed and accurate description of the propagating electromagnetic (EM) field along the cells and their vicinity [8, 9]. We have written and tested our algorithm thoroughly and found it to match perfectly results for light propagation along cones [2].

Images of human glial cells [7, 4] were digitized to define their width as function of depth, at the scale of 0.13

$\mu\text{m}/\text{pixel}$ . The created  $1000 \times 512 \times 512$  data-cube maintains the two characteristic features of the cell: the entrance diameter of the upper funnel cup is  $\sim 12 \mu\text{m}$  and along the light guide,  $\sim 2.4 \mu\text{m}$  [4] (Fig. 2). Further perturbations were added randomly, up to 5% of the radius, and similarly for its center line, in order to simulate the uneven boundaries and undulations of the cells [7, 4]. The cell was divided into four refractive indices, with a smooth transition between them, and the soma was ignored [4], being beside the cell and of lower refractive index. Instead we used for that section the average of the indices above and below the soma.

To account for the scattering and distortion of the various retinal fiber layers, we added random transverse perturbations of the external refractive index on a scale of  $1 \mu\text{m}$  and  $\sim 5\%$  of the local refractive index. Since we do not have a better model of the scattering processes (except to say that no absorption is involved), we employed only measured data: The locations, thicknesses and powers of these regions (NFL, IPL, OPL) were digitized from human retinal cuts [4]. Next another glial cell was appended horizontally with its own uneven edges and bending, but with the same refractive indices. With this setup, we could test both the propagation inside the first cell and the leakage into the next one.

The first step of the simulation was to create a correct light distribution impinging on the cell. The average diffraction pattern from a pupil was approximated by a Gaussian shape, with a width of  $40 \mu\text{m}$ , wider than the input funnel (in most eyes during day time, the width can exceed  $40 \mu\text{m}$  due to monochromatic aberrations). Such a distribution can be created experimentally by collimated pencil beams which are scanned across the pupil [10]. With limited diameter, the role of aberrations is limited, and the EM phase near focus is planar, with tilt rising up to  $10^\circ$ . In our tests, the light distribution was allowed to enter only one cell, and was masked off outside it. Next, the field was propagated down the medium, plane by plane, where every step was of 0.13 micron length. Scattering processes in the cell borders and the surrounding media slowly coupled the field to the neighboring tissue and cells. Then the whole structure was rotated according to the incidence angle and the process was repeated, and again over all wave lengths.

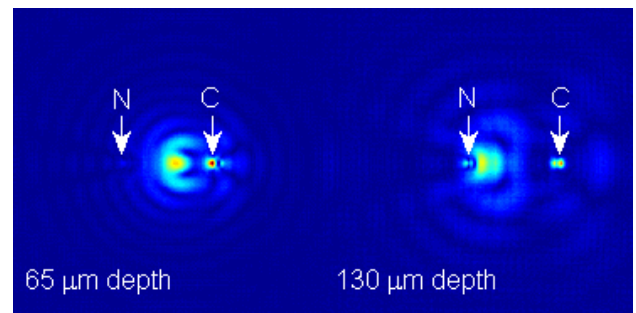


FIG. 4 (Color online). Field distribution half way down the retina (left) and at the photoreceptor layer (right). The tilt angle of the cells is  $6^\circ$  and the wave length is  $0.45 \mu\text{m}$ . The cell locations are marked C and N.

A characteristic field amplitude can be seen in cuts along the cells (Fig. 3), showing an accumulation of intensity in the initial cell and its neighbor, and becoming more defined at the bottom of the cells. In the next step we computed the final intensity by squaring the field matrices. These results are the intensity maintained in the initial cell and the coupled intensity to its nearest neighbor (Fig. 4).

To calculate the transmission of the cells, we integrated the intensity incident on the central cell of area  $\Omega$ ,  $I_i = \iint_{\Omega} |E(\mathbf{r})|^2 d^2\mathbf{r}$ , and the intensities out of the same cell of exit area  $\Phi$ ,  $I_c = \iint_{\Phi} |E(\mathbf{r})|^2 d^2\mathbf{r}$  and the neighbor cell of exit area  $\Xi$ ,  $I_n = \iint_{\Xi} |E(\mathbf{r})|^2 d^2\mathbf{r}$ . The

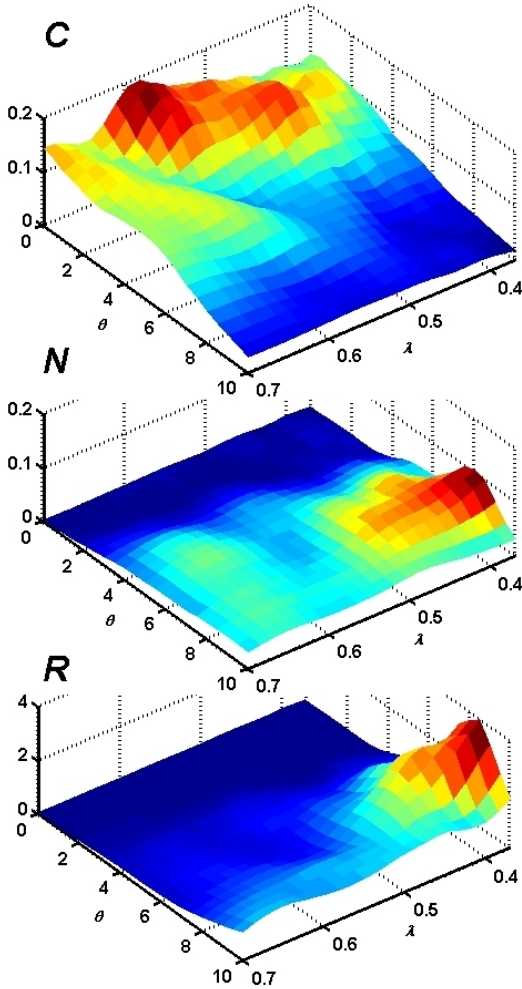


FIG. 5 (Color online). Efficiency of light guiding in the central (top) and coupling to close neighbor glial cell (center): the fraction of light output relative to visible light input for incidence angles corresponding up to fully dilated pupils. Variations in these intensities were  $\sim 5\%$ . The leaked ridge at  $6^0$ - $8^0$  is due to direct propagation of uncaptured light into the neighbor cell. Bottom: the ratio of intensities between the neighbor and the central cell.

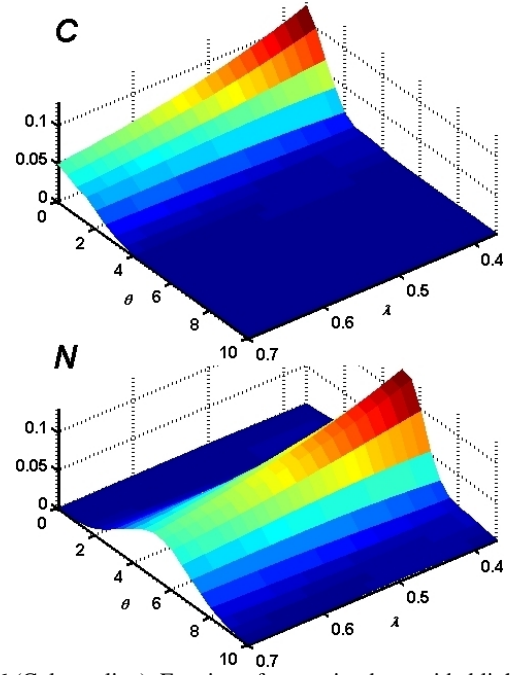


FIG. 6 (Color online). Fraction of transmitted, unguided light, as a function of wave length and incidence angle, at the central cell (top) and the neighbor cell (bottom). Without cells, but still with tissue scattering, the efficiency, angular selectivity and crosstalk drop significantly. Compare to Fig. 5.

efficiency of the central cell was thus  $C = I_c/I_i$ , and the leakage into the neighbor cell was  $N = I_n/I_i$ . This calculation was performed for 23 visible wavelengths and 21 incidence angles, associated with increasingly eccentric entry positions within the pupil [10]. The coupling into the neighbor cell shows (Fig. 5, center) that for small incidence angles (up to  $5^0$ ) the amount of leaked energy is low,  $< 3\%$ . More significant coupling occurred for higher incidence angles. Moreover, for wavelengths in the center of the visible spectrum ( $0.5$ - $0.6 \mu\text{m}$ ), a lower coupling is obtained, even for higher arrival angles. These results are clearer when calculating the ratio of intensities of light at the bottom of the neighbor cell to the guided light at the central cell,  $R = N/C$  (Fig. 5, bottom). The transmission of the various colors was sensitive to deviations of the diameters of the cells from  $2.4 \mu\text{m}$ . If we ignore the glial cells (by equalizing their refractive index to the external tissue), but still include the input mask, less than half the light reaches the central cell, but much more reaches its neighbor (Fig. 6). This comparison shows the enhanced collection efficiency of the glial cells at higher angles. It is also supported by the *in vitro* comparison [4], although the external refractive index there was homogeneous and  $< 1.36$ .

EM striking the retina within a small incidence angle corresponds to a smaller pupil as in day time (photopic) vision. When the pupil is wider (night, or

scotopic, vision), ocular aberrations come into play, and the phase of the resulting EM field is much less regular. Therefore the results provide evidence for a natural optical waveguide array, which preserves almost perfectly images obtained through a narrower pupil. For a wider pupil, in darker conditions, the coupling to the neighbor glial cells is increased but even then mainly for more aberrated eyes and at the edges of the visible spectrum (Fig 5). This inter-cell coupling causes the attached neighbor photoreceptors to be excited as well, and results in loss of resolution of one to two periods of the cone array,  $\sim 20 \mu\text{m}$ .

We considered here light guided down from the glial cell funnel into a single cone at the bottom, as well as into many rods ( $\sim 10$ ). So light not coupled within the central cell can still be sensed by these rods. More data, regarding the scattering power of the different retinal layers, are necessary before the actual distribution of scattered light is calculated. This is clear from Figs. 3 and 4, where light, which was not guided by the glial funnel nor scattered in other retinal tissue, still arrives at the photoreceptor layer, between the glial cell stems and the neighboring cones. We found out that without refractive index fluctuations in the various retinal layers (Fig. 2), even more light reached the region between the cones. This is also evident from the ridge of intensity maxima in the neighbor cell at  $\sim 6^\circ$  in Figs. 5 (center). Notice that this ridge has a minimum at green light, which means that leakage is worse in red and worst in blue. Moreover, it is evident that leakage mainly occurs with dilated pupils for typical cone spacing. However for most cones this crosstalk is of no consequence during day time.

Another notable result is that parafoveal color vision is less affected by chromatic aberrations. The longitudinal chromatic aberration spans the focal spot along the retina, where blue focuses before red. Thus both colors cannot be focused simultaneously on the cones. But with glial light guiding the configuration changes: Regardless of the volume of the focal spot, set by chromatic and monochromatic aberrations [10], the incidence angles are still within our analysis range of a few degrees. That means that they will still be guided by the same glial cell and lead to the same cone. Put the other way around, peripheral light at larger tilt angles will be rejected more readily. This explains why chromatic correction in front of the eye leads to very little improvement in color sensitivity [11]. In most eyes the point spread function is much wider than the glial cell spacing, so neighbor cones of different color sensitivity provide fuller color coverage. In addition, light which arrives at the photoreceptor layer unguided has a higher chance of getting detected by the color-blind rods.

In this study, wave propagation methods allowed us to show that light guiding within the retinal volume is an effective and biologically convenient way to improve the resolution of the eye and reduce chromatic aberration. We also found that the retinal nuclear layers, until now considered a source of distortion, actually improve the decoupling of nearby photoreceptors and thus enhance vision

acuity. Although this study was performed on data from human retinas and eyes, most of its consequences are valid for eyes with other retinal structure and different optics. They are also valid for the more common case of eyes without a central fovea.

Further studies are still required to test the sensitivity of our results to various parameters. While we had no such parameters to vary in the data we used, we can examine the effect of aberrations on the propagated modes: what happens at the far parafovea where aberrations abound, how are colors transmitted, what is the effect of a full glial array at various spacings, or what role does cataract play. We can also quantify how light scattered at the iris and sclera, namely impinging on the retina at higher incidence angles, is rejected by the glial cells to reduce image background. Better data would improve our results: glial cell dimensions, edge smoothness, refractive index and scattering strength. Notice that data from [12] seem not to agree with other measurements [4, 5]. For other animals we can calculate their expected spatial and chromatic acuity.

The fundamental features of the array of glial cells are revealed as an optimal structure designed for preserving the acuity of images in the human retina. It plays a crucial role in vision quality, in humans and in other species.

Parts of this work were supported by Science Foundation Ireland through the Walton Fund and by Israel Science Foundation.

## References

1. G. Westheimer, *Proc. R. Soc. B* **275**, 2777-86 (2008).
2. A. W. Snyder and C. Pask, *Vis. Res.* **13**, 1115-37 (1973).
3. R. Barrer, *J. Opt. Soc. Am.* **47**, 545-55 (1957).
4. K. Franze, J. Grosche, S. N. Skatchkov, S. Schinkinger, C. Foja, D. Schild, O. Uckermann, K. Travis, A. Reichenbach, and J. Guck, *Pub. Nat. Acad. Sci.* **104**, 8287-92, and Supporting Information (2007).
5. C. A. Curcio, K. R. Sloan, R. E. Kalina, and A. E. Hendrickson, *J Comparative Neurology* **292**, 497-523 (1990).
6. S. Somekh, E. Garmire, A. Yariv, H. L. Garvin and R. G. Hunsperger, *Appl. Phys. Lett.* **22**, 46-7 (1973).
7. T. I. Chao, J. Grosche, K. J. Friedrich, B. Biederman, M. Francke, T. Pannicke, W. Reichelt, M. Wulst, C. Muehle, S. Pritz-Hohmeier, H. Kuhrt, F. Faud, W. Drommer, M. Kasper, E. Buse and A. Reichenbach, *J. Neurocyt* **26**, 439-54 (1997).
8. J. Van Roey, J. Van der Donk, and P.E Lagasse, *J. Opt. Soc. Am.* **71**, 803-10 (1981).
9. K. Okamoto, *Fundamentals of optical waveguides*, Elsevier (2006).
10. B. Vohnsen, I. Iglesias, and P. Artal, *J. Opt. Soc. Am. A* **22**, 2318-28 (2005).
11. Y. Benny, S. Manzanera, P. M. Prieto, E. N. Ribak and P. Artal, *J. Opt. Soc. Am. A* **24**, 1538-44 (2007).
12. S. Nishikawa and M. Tamai, *Current Eye Research* **22**, 34-41 (2001).